Partially fluorinated MIL-47 and Al-MIL-53 frameworks: influence of functionalization on sorption and breathing properties†

Shyam Biswas,[a] Tom Rémy,[b] Sarah Couck,[b] Dmytro Denysenko,[c] Geert Rampelberg,[d] Joeri F. M. Denayer,[b] Dirk Volkmer,[c] Christophe Detavernier[d] and Pascal Van Der Voort*[a]

Two perfluorinated metal hydroxo terephthalates $[M^{III}(OH)(BDC\text{-}F)]\cdot n(guests)$ (M^{III} = V, MIL-47-F-AS or **1-AS**; Al, Al-MIL-53-F-AS or **2-AS**) (BDC-F = 2-fluoro-1,4-benzenedicarboxylate; AS = as-synthesized) have been synthesized by a hydrothermal method using microwave irradiation (**1-AS**) or conventional electric heating (**2-AS**), respectively. The unreacted or occluded H_2BDC-F molecules can be removed under vacuum by direct thermal activation or exchange of guest molecules followed by thermal treatment leading to the empty-pore forms of the title compounds $[V^{IV}(O)(BDC\text{-}F)]$ (MIL-47-F, **1**) and $[Al^{III}(OH)(BDC\text{-}F)]$ (Al-MIL-53-F, **2**). Thermogravimetric analysis (TGA) and temperature-dependent XRPD (TDXRPD) experiments indicate that the compounds are stable up to 385 and 480 °C, respectively. Both of the thermally activated compounds exhibit significant microporosity, as verified by N_2, CO_2, *n*-hexane, *o*- and *p*-xylene sorption analyses. The structural changes of **2** upon adsorption of CO_2, *n*-hexane, *o*- and *p*-xylene were highly influenced due to functionalization by –F groups, as compared to parent Al-MIL-53. The –F groups also introduce a certain degree of hydrophobicity into the frameworks, as demonstrated by the H_2O sorption analyses.

Introduction

Metal–organic frameworks (MOFs),[1–3] which are a fascinating class of highly crystalline and nanoporous materials, have been the subject of tremendous research interest over the past few years owing to their intriguing structural topologies and promising applications in a wide range of areas such as gas storage/separation,[4–6] catalysis[7,8] and drug delivery.[9–12] Built up from inorganic building units and polytopic organic linkers, MOFs show similarity with zeolites in terms of porosity. In sharp contrast to zeolites, the modular character of MOFs allows the systematic tuning of the pore features (dimensions or surface property) by varying the metal ions or by attaching functional groups (having different dimensions, polarities, hydrophilicities, acidities, *etc.*) to the organic linker, without altering the underlying topology of the framework. In the latter case, the functional groups can be introduced to the organic moiety (i) by directly using pre-functionalized linkers during synthesis or (ii) by a post-synthetic modification approach.[13] Both strategies have been successfully employed for functionalization of rigid as well as flexible (often denoted as "breathing"[14]) MOFs. The functionalization of rigid MOFs affects their sorption[15–19] and selectivity[20,21] as well as thermal and chemical stability.[22] In addition to changing these properties, the functionalization of flexible MOFs can influence their breathing behaviour (*i.e.* probability, nature and magnitude of pore opening/closing).[23–26]

Among the various porous MOFs known to date, the terephthalate based MOFs MIL-47(V^{IV})[27] (MIL = Material of the Institut Lavoisier) and M-MIL-53 (M^{III} = Al,[28] Cr,[29] Fe,[30] Ga[31]) are very promising materials for various applications.[32]

[a] *Dept. of Inorganic and Physical Chemistry, Centre for Ordered Materials, Organometallics and Catalysis, Ghent University, Krijgslaan 281-S3, 9000 Ghent, Belgium. E-mail: pascal.vandervoort@ugent.be; Fax: +32 9 264 49 83; Tel: +32 964 44 42*

[b] *Department of Chemical Engineering, Vrije Universiteit Brussel, Pleinlaan 2, 1050 Brussel, Belgium*

[c] *Institute of Physics, Chair of Solid State and Material Science, Augsburg University, Universitätsstrasse 1, 86135 Augsburg, Germany*

[d] *Department of Solid State Sciences, Ghent University, Krijgslaan 281-S1, 9000 Ghent, Belgium*

† Electronic supplementary information (ESI) available: Additional ambient and temperature-dependent XRPD patterns, DRIFT and Raman spectra, tables containing results of TG, DRIFT and elemental analyses. See DOI: 10.1039/c3cp44204g

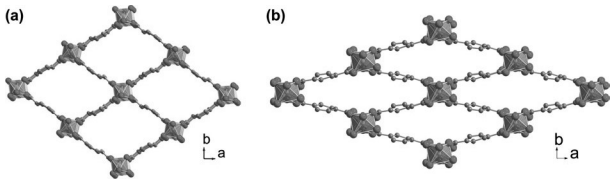

Fig. 1 Ball-and-stick representations (viewed along the crystallographic c-axis) of the 3D framework structure of (a) a large pore (LP) form of Al-MIL-53 and (b) a narrow pore (NP) form of Al-MIL-53. Metal atoms are displayed as octahedra. The hydrogen atoms and guest molecules have been removed from all structural plots for clarity. The figure was drawn using atomic coordinates provided in ref. 28.

These solids are built up from infinite *trans* chains of corner-sharing $[V^{IV}O_6]$ or $[M^{III}O_4(OH)_2]$ octahedra interconnected by terephthalate linkers to form one-dimensional rhombic-shaped channels (Fig. 1). The materials have the general chemical composition [M(X)(BDC)] (X = OH, M = Al^{III} for Al-MIL-53 and X = O, M = V^{IV} for MIL-47(V^{IV}); BDC = 1,4-benzenedicarboxylate). The presence of μ_2-OH groups has been shown to control the flexibility of M-MIL-53 upon adsorption of guest molecules, whereas their absence in MIL-47(V^{IV}) leads to a rigid framework regardless of the nature of the stimulus. The reversible structural flexibility of M-MIL-53 depends strongly on the framework metal ion,[31,33] size and functionality of the linker molecules,[24] temperature,[31,33] adsorbate pressure[26] as well as the nature of the guest molecules.[28,29] Therefore, detailed investigations of the breathing properties have been carried out with different gases/vapors such as CO_2,[29,34–41] linear alkanes,[42–47] or xylenes[48,49] as the guest molecules. Either a narrow pore (NP) or a large pore (LP) form is observed depending on the above-mentioned parameters and the reversible transition between the two forms can result in a change in unit cell volume up to 40%.[24] Recently, a special thermal activation procedure under vacuum has been developed to obtain the activated LP form (denoted as MIL-47(V^{III})) having the formula $[V^{III}(OH)(BDC)]$ that can transform to a hydrated narrow pore (NP) form upon cooling down to room temperature.[50] More recently, MIL-47(V^{IV}) has also been shown to change to a NP form under high mechanical pressure.[51]

Fluorinated MOFs (FMOFs) show increase in the following properties: (i) moisture stability,[52] (ii) H_2 adsorption enthalpy[53–58] and (iii) hydrocarbon adsorption.[59] However, only a handful of examples of fluorinated MOFs[52–61] have been reported to date. It has been concluded that the enhancement of H_2 adsorption due to fluorination in MOFs is not a universal phenomenon, but can vary from system to system.[56,57] Most remarkably, no detectable water adsorption even at near 100% relative humidity has been observed for a Ag(I)-based MOF incorporating 3,5-bis(trifluoromethyl)-1,2,4-triazolate, which shows high capacity with high affinity to C_6–C_8 hydrocarbons of oil components.[59]

Al-based MOFs are advantageous over other MOFs owing to their light weight, non-toxicity and enhanced stability against hydrolysis.[62–64] Therefore, a wide variety of functionalized Al-MIL-53-X (X = $-NH_2$, –OH, $-CO_2H$, $-(CO_2H)_2$, $-C_6H_4$, –Cl, –Br, $-CH_3$, $-NO_2$, $-(OH)_2$)[23,40,65–70] compounds have been reported. On the other hand, MIL-47 is unstable in water, though it has been shown to (selectively) adsorb significant amounts of linear hydrocarbons[45–47] and xylene isomers.[71,72]

Encouraged by the advantages of fluorinated MOFs, and those of Al- and V-based MOFs, we have synthesized and thoroughly characterized two partially fluorinated MOFs, namely MIL-47-F and Al-MIL-53-F. In this article, we wish to report the influence of fluorination on the gas/vapor sorption and breathing properties of the two perfluorinated MOFs.

Experimental

Materials and general methods

The H_2BDC-F ligand was synthesized as described previously.[73] All other starting materials were of reagent grade and used as received from the commercial supplier. VCl_3 was weighed in a nitrogen-filled glove box. The thermally activated MIL-47-F (**1**) was also stored in a glove box because of its air-sensitivity. All other manipulations were carried out under an air atmosphere. Diffuse-reflectance infrared Fourier transform (DRIFT) spectra were recorded using a Thermo Nicolet 6700 FTIR spectrometer equipped with a nitrogen-cooled MCT detector and a KBr beam splitter. The DRIFT cell was connected to a vacuum manifold. The following indications are used to characterize absorption bands: very strong (vs), strong (s), medium (m), weak (w), shoulder (sh), and broad (br). The Raman spectrum was collected using a RXN1 Raman spectrometer (Kaiser Optical Systems) fitted with a 532 nm laser operating at 40 mW using an optical probe. Elemental analyses (C, H, N) were carried out using a Thermo Scientific Flash 2000 CHNS-O analyzer equipped with a TCD detector. Thermogravimetric analysis (TGA) was performed using a Netzsch STA-409CD thermal analyzer in a temperature range of 25–600 °C under an air atmosphere at a heating rate of 2 °C min^{-1}. Ambient temperature X-ray powder diffraction (XRPD) patterns were recorded using a Thermo Scientific ARL X'Tra diffractometer operated at 40 kV, 40 mA with Cu-Kα (λ = 1.5406 Å) radiation. High resolution *in situ* synchrotron XRPD patterns of **2** as a function of CO_2 pressure were collected at beamline I11 of Diamond Light Source (Didcot, UK) by using multi-analysing crystal-detectors (MACs) and a monochromatic beam with a wavelength of 0.827131 Å. The well-ground powder sample of the thermally activated form of **2** was filled in a 0.5 mm glass capillary. A gas dosing system was used to admit CO_2 from vacuum to 2.5 bar of pressure into the capillary filled with the sample and exposed to the X-ray beam. Prior to the measurement, the sample was degassed at 200 °C for 30 min (heating rate: 5 °C min^{-1}) under vacuum. The *in situ* XRPD data upon CO_2 dosing were collected at −40 and −80 °C. The temperature was controlled by an Oxford Cryostream Cooler. A typical data set at each pressure point was collected. The XRPD patterns of **2** at −80 °C immediately after evacuation and after 5 h of staying at this temperature under vacuum were selected for the determination of lattice parameters of LP and NP phases, respectively. Lattice parameters were determined by using either

TREOR[74] or DICVOL[75] program and refined with the STOE's WinXPow software[76] package. Temperature-dependent XRPD patterns were collected using a Bruker D8 Discover X-ray diffractometer with a linear detector; the XRD patterns were recorded from room temperature to 800 °C (**1**) or 650 °C (**2**) with a temperature ramp of 0.1 °C s^{-1} (**1**) or 0.02 °C s^{-1} (**2**) in air flow. The nitrogen sorption isotherms up to 1 bar were measured by using a Belsorp Mini apparatus at −196 °C. The low pressure carbon dioxide adsorption analysis was performed using a Belsorp Max instrument combined with the BELCryo system at −78.3 °C. The high-pressure carbon dioxide sorption isotherms were recorded using a volumetric HPA-100 device from VTI Corporation at 30 °C. The vapor phase isotherms of *n*-hexane, *o*- and *p*-xylene were measured by the gravimetric method using a microbalance of VTI Corporation. The compounds were degassed (**1**: 100 °C, 1 h; **2**: 150 °C, 16 h) under dynamic vacuum prior to the sorption experiments.

MIL-47 (ref. 27) and Al-MIL-53 (ref. 28 and 45) were synthesized and activated according to literature methods. The usual characterization experiments (XRPD, TGA, IR spectroscopy, and sorption analysis) were performed to confirm their purity.

Syntheses

$[V(OH)(C_8H_3FO_4)]\cdot 0.3(C_8H_5FO_4)$ (MIL-47-F-AS) (1-AS). A mixture of VCl_3 (100 mg, 0.64 mmol) and H_2BDC-F (117 mg, 0.64 mmol) in 2 mL of water was placed in a Pyrex tube (10 mL). The tube was sealed and heated in a microwave synthesizer (CEM, Discover S) to 170 °C at 150 W, held under these conditions for 30 min with stirring, then cooled to room temperature. The greenish yellow precipitate was collected by filtration, and dried in air. The yield was 120 mg (0.39 mmol, 58%). Elemental analysis calcd for $C_{10.4}H_{5.5}F_{1.3}O_{6.2}V$ (305.29 g mol^{-1}): C 40.91, H 1.81; found: C 41.30, H 1.62%. DRIFT (KBr, cm^{-1}): 3605 (m), 2662 (br), 2544 (br), 1706 (s), 1627 (w), 1580 (vs), 1500 (s), 1420 (vs), 1390 (vs), 1287 (m), 1231 (m), 1091 (w), 958 (sh), 915 (s), 831 (w), 795 (w), 768 (s), 758 (sh), 685 (w).

$[Al(OH)(C_8H_3FO_4)]\cdot 0.5(C_8H_5FO_4)$ (Al-MIL-53-F-AS) (2-AS). A mixture of $AlCl_3\cdot 6H_2O$ (0.5 g, 2.07 mmol), H_2BDC-F (0.38 g, 2.07 mmol), and water (25 mL) was placed in a 100 mL Teflon liner, and the resulting mixture was heated in a conventional oven at 210 °C for 24 h and cooled to room temperature. The white precipitate was collected by filtration, and dried in air. The yield was 0.47 g (1.47 mmol, 72%). Elemental analysis calcd for $C_{12}H_{6.5}AlF_{1.5}O_7$ (318.15 g mol^{-1}): C 45.30, H 2.05; found: C 45.40, H 2.12%. DRIFT (KBr, cm^{-1}): 3679 (m), 2982 (br), 2866 (br), 2664 (br), 2543 (br), 1708 (vs), 1619 (vs), 1574 (w), 1501 (s), 1428 (vs), 1399 (s), 1285 (m), 1234 (m), 1100 (w), 1011 (s), 963 (w), 944 (w), 899 (m), 845 (w), 807 (w), 775 (s), 756 (m), 654 (m).

Activation of the compounds

Compound **1-AS** was directly heated at 340 °C for 12 h under dynamic vacuum to obtain the evacuated form of the compound.

Compound **2-AS** was activated in two steps. A suspension of **2-AS** was heated in *N,N′*-dimethylformamide (30 mL) at 155 °C for 24 h in a conventional oven. The filtered solid (denoted as **2-DMF**) was heated at 250 °C under dynamic vacuum for 24 h to get the activated form of **2**.

Results and discussion

Syntheses and activation

Compounds **1** and **2** have been prepared under hydrothermal conditions by using microwave irradiation or conventional electric heating, respectively. The starting aqueous reaction mixtures consisted of MCl_3 (M = V, **1**; Al, **2**) and H_2BDC-F linker present in a molar ratio of 1 : 1. The time required for the syntheses of **1** and **2** differs significantly with respect to the ones reported previously for the unmodified MIL-47 (ref. 27) and Al-MIL-53.[28] Compared to the several days (MIL-47: 4 d, Al-MIL-53: 3 d) of synthesis time used for the pristine solids, **1** and **2** have been synthesized in only 30 min and 1 d, respectively. It is worth noting that the microwave irradiation route has been formerly applied to synthesize five isostructural and functionalized MIL-47-X (X = $-C_4H_4$, $-(OH)_2$, $-(CH_3)_2$, $-Cl_4$ and $-Br_4$) compounds.[77]

The AS-forms of the two compounds contain non-coordinated H_2BDC-F linker molecules encapsulated within the pores which were removed by direct thermal treatment (**1-AS**) under vacuum or in a two-step procedure (**2-AS**). For the latter compound, the guest molecules were exchanged by heating the AS compounds with a polar solvent such as *N,N′*-dimethylformamide (DMF). In the second step, the DMF molecules were removed by heating the guest-exchanged compound under dynamic vacuum. After cooling to room temperature, the activated **2** adsorbs different amounts of water from air depending on the exposure time.

DRIFT and Raman analysis

In the DRIFT spectra (Fig. S1 and S2, ESI†) of AS forms of the two compounds, the strong absorption bands due to asymmetric and symmetric $-CO_2$ stretching vibrations of the coordinated terephthalate linker molecules are located in the regions 1565–1615 cm^{-1} and 1420–1430 cm^{-1}, respectively.[28] The additional strong absorption bands at *ca.* 1710 cm^{-1}, observed in the DRIFT spectra of AS forms of the compounds, can be attributed to the protonated form ($-CO_2H$) of unreacted or guest BDC-F linker molecules.[28] The absorption bands of the occluded H_2BDC-F molecules are absent in the DRIFT spectra of empty-pore forms of the two compounds, suggesting complete activation. The characteristic strong absorption band of the carbonyl stretching vibration of guest DMF molecules appears at 1681 cm^{-1} in the DRIFT spectra of **2-DMF**. The stretching vibration of the μ_2-OH group exhibits medium absorption bands in regions 3600–3680 cm^{-1} in the DRIFT spectra of **1-AS**, **2-AS**, **2-DMF** and **2**.[24] This band is absent in the DRIFT spectrum of the empty-pore form of **1**, indicating the absence of μ_2-OH group in this compound.

Raman analysis (Fig. S3, ESI†) was performed in order to determine the oxidation state of the vanadium atom in the thermally activated **1**. The stretching vibration of the V^{IV} = O group is observed at *ca.* 900 cm^{-1} for activated **1**, which verifies

that the V^{III}–OH group is oxidized to V^{IV} = O during the thermal treatment.

Structure description

The refined lattice parameters (Table 1) of the different forms of **1** and **2** determined from their laboratory and synchrotron XRPD patterns collected under ambient conditions are similar to the un-functionalized MIL-47 (ref. 27) and Al-MIL-53,[28] respectively. The different forms of **1** and **2** are thus isostructural with MIL-47 and Al-MIL-53, respectively, also revealed from the similarity between their XRPD patterns (Fig. S4 and S5, ESI†). Moreover, the framework topologies of MIL-47 and Al-MIL-53 (Fig. 1) are identical. As described by Férey's group, the 4^4 net of the AS forms of MIL-47 (ref. 27) and Al-MIL-53 (ref. 28) contain infinite tilted *trans* chains of corner-sharing (*via* μ_2-OH group) $[M^{III}O_4(OH)_2]$ (M = V, **1**; Al, **2**) octahedra, which are interconnected by the carboxylate groups of the BDC linkers to form a three-dimensional framework possessing one-dimensional (1D) rhombic-shaped pores. In the AS-forms of the fluorinated compounds, the 1D channels are occupied by guest H_2BDC-F linker molecules under ambient conditions. The guest molecules are removed by thermal activation leading to the empty-pore forms of the compounds. During thermal activation of **1-AS**, the framework V^{III} ions are oxidized to V^{IV} and the V–OH bonds are changed to a vanadyl (V^{IV} = O) group, but the topology of the framework remains unchanged. In contrast, the aluminum atoms of **2-AS** still retain their +3 oxidation state after thermal activation. Depending on both the nature of guest molecules and the temperature, the framework of **2** shows either a narrow pore (NP; crystal system: monoclinic; unit cell volume: ~1000 Å^3) or a large pore (LP; crystal system: orthorhombic; unit cell volume: ~1300–1400 Å^3) form (Fig. 1, Table 1 and *in situ* synchrotron XRPD analysis section). On the other hand, the unit cell volumes (Table 1) of **1-AS** and **1** differ slightly and both of them correspond to the LP form (crystal system: orthorhombic; unit cell volume: ~1500–1600 Å^3). Thus, the temperature does not induce significant structural change in **1** as compared with **2**. Noticeably, the thermally activated LP form of **2** upon adsorption of water from air also exhibits a LP form (Table 1), which is contrary to unfunctionalized Al-MIL-53 (ref. 28) and other functionalized Al-MIL-53-X (X = –Cl, Br, $–CH_3$, $–NO_2$, $–NH_2$, $–CO_2H$, $–(OH)_2$).[23,66,70]

Thermal stability

To examine the thermal stability of **1** and **2**, thermogravimetric analyses (TGA) were performed on the different forms of the compounds in an air atmosphere. On the basis of the TG analyses, **1** and **2** are thermally stable up to 385 and 480 °C, respectively. The thermal stabilities of the two partially fluorinated compounds are comparable to that of unfunctionalized MIL-47 (400 °C) or Al-MIL-53 (500 °C). Noticeably, **2** possesses higher thermal stability compared to **1**, in spite of having the same framework topology.

In the TG curves of the AS and DMF-exchanged forms of the compounds (Fig. 2), any weight loss step that occurs below the decomposition temperature of the frameworks can be assigned to the removal of the guest H_2BDC-F linker and

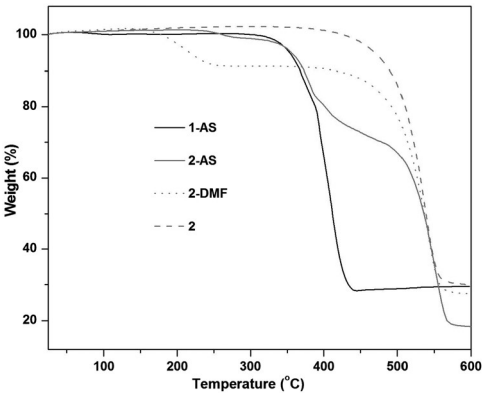

Fig. 2 TG curves of as-synthesized **1** (black, solid line), as-synthesized **2** (grey, solid line), DMF-exchanged **2** (grey, dotted line) and thermally activated **2** (grey, dashed line) recorded in an air atmosphere.

Table 1 Molecular formulae, refined lattice parameters[a] and pore types[b] of the different forms of **1**, **2**, MIL-47 and Al-MIL-53

Compound	Molecular formula	*a* (Å)	b (Å)	*c* (Å)	*V* (Å^3)	*β*(deg)	Pore type
1-AS	$[V^{III}(OH)(BDC\text{-}F)]\cdot 0.3(H_2BDC\text{-}F)$	17.51(5)	12.275(14)	6.881(10)	1478.7(64)		LP
MIL-47-AS[27]	$[V^{III}(OH)(BDC)]\cdot 0.75(H_2BDC)$	17.5185(11)	12.1680(8)	6.8750(4)	1465.51(16)		LP
1	$[V^{IV}(OH)(BDC\text{-}F)]$	16.406(7)	13.824(9)	6.870(3)	1557.9(15)		LP
MIL-47 (ref. 27)	$[V^{IV}(O)(BDC)]$	16.143(3)	13.939(2)	6.8179(12)	1534.1(5)		LP
2-AS	$[Al(OH)(BDC)]\cdot 0.5(H_2BDC\text{-}F)$	17.01(3)	12.376(11)	6.630(11)	1395.6(49)		LP
Al-MIL-53-AS[28]	$[Al(OH)(BDC)]\cdot 0.7(H_2BDC)$	17.129(2)	12.182(1)	6.628(1)	1383.1(2)		LP
2-DMF	$[Al(OH)(BDC\text{-}F)]\cdot 3(DMF)$	17.85(11)	11.04(39)	6.58(6)	1297.3(48)		LP
Al-MIL-53-DMF[23]	$[Al(OH)(BDC)]\cdot 1.1(DMF)$	17.55(6)	11.396(17)	6.615(13)	1322.8(74)		LP
2 (hydrated)[c]	$[Al(OH)(BDC\text{-}F)]\cdot xH_2O$	17.327(9)	12.205(7)	6.656(3)	1471.0(17)		LP
2 (dehydrated)	$[Al(OH)(BDC\text{-}F)]$	16.7821(6)	12.731(8)	6.627(14)	1416.05(21)		LP
		19.599(6)	8.202(15)	6.610(5)	1020.9(23)	106.11(7)	NP
Al-MIL-53 (hydrated)[c,28]	$[Al(OH)(BDC)]\cdot 1.0(H_2O)$	19.513(2)	7.612(1)	6.576(1)	946.8(1)	104.24(1)	NP
Al-MIL-53 (dehydrated)[d,28]	$[Al(OH)(BDC)]$	16.675(3)	12.813(2)	6.6085(9)	1411.9(4)		LP

[a] Lattice parameters were determined from laboratory XRPD data (λ = 1.5406 Å) collected at room temperature, except **2** (dehydrated) for which lattice parameters for the LP and the NP phases were collected from *in situ* synchrotron XRPD data (λ = 0.827131 Å) at −80 °C immediately after evacuation and after 5 h of staying at this temperature under vacuum, respectively. [b] LP: large pore, NP: narrow pore. [c] Refers to the forms of **2** and Al-MIL-53 after adsorption of variable amounts of water from air when the thermally activated compounds are cooled to room temperature. [d] Refers to the so-called high-temperature (HT) form of Al-MIL-53.

DMF molecules, respectively. Below the decomposition temperature, the thermally activated form of **2** does not display any weight loss step, indicating relatively more hydrophobicity of the compound as compared with the other known functionalized Al-MIL-53-X (X = –Cl, Br, $–CH_3$, $–NO_2$, $–NH_2$, $–CO_2H$, $–(OH)_2$)[23,66,70] compounds. The activated forms of the previously reported Al-MIL-53-X compounds were found to adsorb different amounts of water from air depending on the attached functional groups. For the different forms of **1** and **2**, the observed weight losses are consistent with the calculated ones as well as the elemental analyses (Table S1 and S2, ESI†), indicating phase purity of the compounds.

The high thermal stability of the compounds has also been verified by temperature-dependent XRPD (TDXRPD) measurements. According to the TDXRPD patterns (Fig. S6 and S7, ESI†), the AS form of **1** and the thermally activated form of **2** are stable up to 460 and 560 °C, respectively. It should be noted that the thermal stabilities obtained from the TDXRPD measurements (6 °C min^{-1}, **1**; 1.2 °C min^{-1}, **2**) cannot be compared with those observed in TG analyses (2 °C min^{-1}) due to the employment of different heating rates in the two types of measurements.

Gas/vapor sorption properties

In order to verify the effect of functionalization by –F groups on the sorption and breathing properties, CO_2, *n*-hexane, *o*-/*p*-xylene and H_2O sorption analyses were carried out on the thermally activated **1** and **2**.

The N_2 sorption measurements performed on the thermally activated **1** and **2** reveal type-I adsorption isotherms (Fig. 3). The micropore volumes (Table 2) derived from the N_2 adsorption isotherms exhibit considerable porosities, which are lower than the ones reported for unfunctionalized MIL-47 (ref. 27) and Al-MIL-53.[28]

The high pressure CO_2 sorption analyses carried out on the thermally activated **1** and **2** at 30 °C show type-I isotherms (Fig. 4). Surprisingly, no hysteresis loop was observed in the high pressure CO_2 sorption isotherms of the aluminum-based **2**, even when the measurement temperature was lowered to −10 °C (data not shown here). This phenomenon is in sharp contrast to parent Al-MIL-53,[41] for which a distinct hysteresis loop was observed in the high pressure CO_2 adsorption–desorption isotherms at 31 °C. Thus, the attached fluorine atoms play an important role in determining the temperature region for the structural transformation of **2**. In the next section, we show by *in situ* synchrotron XRPD measurements (Fig. 8b) that the expected structural transition of **2** indeed takes place upon adsorption of CO_2 when the temperature is further lowered to −40 or −80 °C. Moreover, the low-pressure CO_2 sorption analysis (Fig. 5) performed on the thermally

Table 2 Specific Langmuir surface areas and micropore volumes of the MIL-47-X compounds determined from N_2 adsorption isotherms

Compound	Specific Langmuir surface area[a] (m^2 g^{-1})	Micropore volume[b] (cm^3 g^{-1})
1	1078	0.36
2	1137	0.48
MIL-47	1222	0.38
Al-MIL-53	1590	0.55

[a] The specific Langmuir surface areas have been calculated from the N_2 adsorption isotherms. [b] The micropore volumes have been calculated at $p/p_0 = 0.5$.

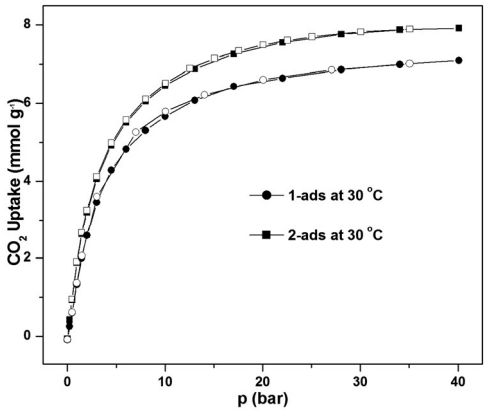

Fig. 4 High pressure CO_2 adsorption (closed symbols) and desorption (open symbols) isotherms of the thermally activated **1** (circles) and **2** (squares) measured at 30 °C.

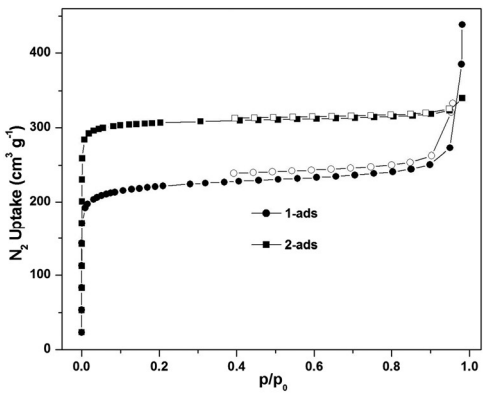

Fig. 3 Low pressure N_2 adsorption (closed symbols) and desorption (open symbols) isotherms of the thermally activated **1** (circles) and **2** (squares) recorded at −196 °C.

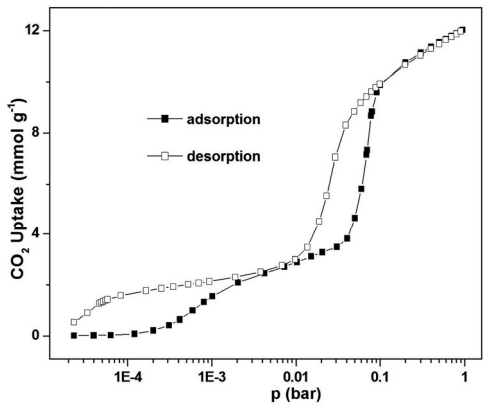

Fig. 5 Low pressure CO_2 adsorption (closed symbols) and desorption (open symbols) isotherms of the thermally activated **2** measured at −78.3 °C (logarithmic scale).

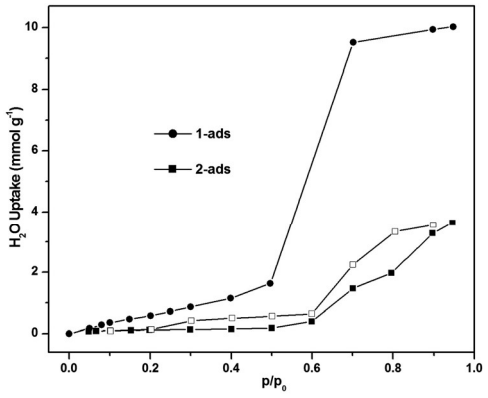

Fig. 6 H_2O adsorption (closed symbols) and desorption (open symbols) isotherms of the thermally activated **1** (circles) and **2** (squares) measured at 50 °C.

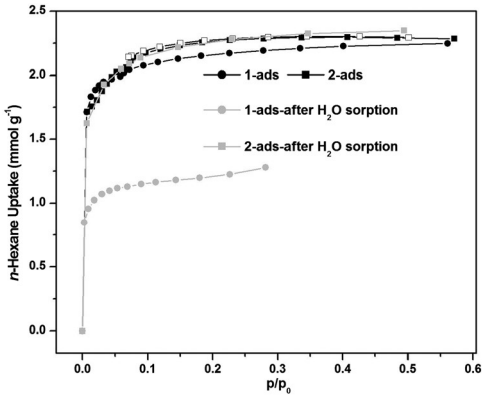

Fig. 7 *n*-Hexane adsorption (closed symbols) and desorption (open symbols) isotherms of the thermally activated **1** (circles) and **2** (squares) measured at 50 °C. Adsorption isotherms of the reactivated **1** and **2** recovered from the H_2O sorption isotherms are shown as grey circles and squares, respectively.

activated **2** at −78.3 °C up to 1 bar reveals two distinct hysteresis loops, corresponding to the LP → NP and NP → LP transitions in the lower and higher pressure range, respectively. The occurrence of two hysteresis loops has previously been observed for parent Al-MIL-53 in Xe and CH_4 sorption isotherms at −53 and −49 °C, respectively.[78,79] The CO_2 adsorption capacity at 30 °C and 25 bar reaches 6.8 and 7.7 mmol g^{-1} for **1** and **2**, respectively, which are lower compared to the value (∼10.5 mmol g^{-1})[41] observed for both un-modified MIL-47 and Al-MIL-53 at 31 °C and 25 bar. Upon lowering the temperature to −78.3 °C, the CO_2 uptake value of **2** at 1 bar rises to 12.0 mmol g^{-1}.

In order to verify the expected hydrophobicity due to the introduction of –F groups, H_2O sorption experiments (Fig. 6) were performed on the thermally activated **1** and **2** at 50 °C. Indeed, both **1** and **2** display low adsorption capacity (<1 mmol g^{-1}) for H_2O below p/p_0 values of 0.4 and 0.6, respectively. After that, the H_2O uptake values of **1** and **2** rise steeply and finally reach to 10 and 3.7 mmol g^{-1}, respectively, at p/p_0 = 0.9. The H_2O adsorption isotherm of **1** can be classified as a type-V isotherm,[80] which has rarely[81,82] been observed in other MOFs. The H_2O adsorption capacity of the aluminum-based **2** at p/p_0 = 0.9 lies below the range of other (–Cl, –Br, $-CH_3$, $-NO_2$, $-NH_2$: ∼5–10 mmol g^{-1}, $-(OH)_2$: 24.3 mmol g^{-1})[23] functionalized Al-MIL-53 compounds. As verified by the XRPD analysis of the samples recovered from the H_2O sorption measurements, **1** decomposes upon prolonged contact with H_2O, whereas **2** maintains its structural integrity in the presence of H_2O. The thermally activated forms of MIL-47 and Al-MIL-53 are known to be hydrophobic and hydrophilic, respectively. As a proof of principle, here we show that a certain amount of hydrophobicity can be introduced into the Al-MIL-53 framework through the attachment of one hydrophobic –F functionality per terephthalate linker molecule. It is noteworthy that water-repellent $-CH_3$ and $-OCF_3$ groups have been formerly introduced at the organic linker of Zn-based MOFs in order to make them highly water-resistant.[52,83]

MIL-47 and Al-MIL-53 have been previously reported to exhibit large uptakes for hydrophobic gas/vapor molecules such as *n*-hexane[42–47] and *o*-/*p*-xylene.[48,49,71,72] Inspired by the intrinsic hydrophobicity of MIL-47 and the additional hydrophobicity introduced through the incorporation of –F groups in the frameworks of **1** and **2**, we have measured *n*-hexane and *o*-/*p*-xylene sorption isotherms for the two compounds at 50 and 70 °C, respectively.

The *n*-hexane sorption isotherms (Fig. 7) of **1** and **2** display type-I isotherms. In the *n*-hexane sorption isotherm of **2**, no sub-step is observed, which is contrary to parent Al-MIL-53.[45] Thus, the incorporated hydrophobic –F groups suppress the structural transition of **2** upon the adsorption of *n*-hexane. The *n*-hexane adsorption capacity of **1** and **2** at 50 °C and p/p_0 = 0.5 reaches 2.3 mmol g^{-1} for each compound, which is comparable to that of pristine MIL-47 (2.0 mmol g^{-1})[46] and Al-MIL-53 (2.9 mmol g^{-1}).[45] The *n*-hexane adsorption isotherm measured on the sample of **1** recovered from the H_2O sorption analysis shows lower uptake compared to the untreated (H_2O) sample. On the other hand, the *n*-hexane uptake of the sample of **2** recovered from the H_2O sorption measurement exhibits similar values as the untreated (H_2O) sample. These facts suggest that **1** collapses while **2** retains its structural integrity after the water sorption experiment.

The *o*-xylene sorption isotherms (Fig. 8) of both **1** and **2** show type-I behaviour. No hysteresis loop is observed in the *o*-xylene

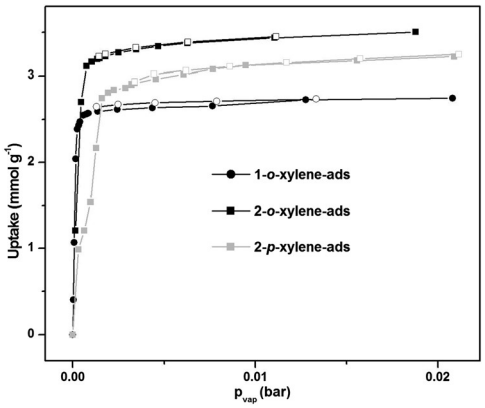

Fig. 8 *o*- and *p*-Xylene adsorption (closed symbols) and desorption (open symbols) isotherms of the thermally activated **1** (circles) and **2** (squares) measured at 70 °C.

Table 3 *o*- and *p*-Xylene uptake values of **1**, **2**, MIL-47 and Al-MIL-53 at 0.02 bar and different temperatures

Compound	Type of xylene isomer	Uptake (mmol g^{-1})	Temperature (°C)
1	*o*-Xylene	2.7	70
2	*o*-Xylene	3.5	70
	p-Xylene	3.2	
MIL-47 (ref. 71)	*o*-Xylene	3.5	70
	p-Xylene	3.7	
Al-MIL-53 (ref. 49)	*o*-Xylene	4.1	110
	p-Xylene	3.3	

adsorption–desorption isotherms of **2**, which is in sharp contrast with unfunctionalized Al-MIL-53.[49] For the latter compound, the adsorption isotherms of *p*- and *m*-xylene consist of large hysteresis loops encompassing a relatively broad range (p/p_0 = 0.005–0.02) as compared to *o*-xylene. A small hysteresis loop in the *o*-xylene adsorption isotherm of parent Al-MIL-53 is noticed below a p/p_0 of 0.005. Interestingly, a minor hysteresis loop is also present in the *p*-xylene adsorption isotherm of **2** below a p/p_0 of 0.005. Thus, **2** exhibits a different breathing feature upon adsorption of *o*- and *p*-xylene as compared to Al-MIL-53. The *o*- and *p*-xylene adsorption capacities (Table 3) of **1** and **2** at 70 °C and 0.02 bar are comparable to those of MIL-47 (ref. 71) and Al-MIL-53.[49]

In situ synchrotron XRPD analysis

As mentioned in the gas/vapor sorption properties section, **2** does not show any structural change upon adsorption of CO_2 even at −10 °C up to a pressure of 25 bar. We suspected that the structural transformation of **2** might occur at a temperature lower than −10 °C, and therefore we decided to collect *in situ* synchrotron XRPD patterns (Fig. 9 and S8, ESI†) of **2** at −40 and −80 °C as a function of CO_2 pressure. The refined lattice parameters collected from the *in situ* synchrotron XRPD patterns are summarized in Table 1.

At −80 °C under vacuum, the Bragg reflections in the XRPD pattern of **2** (Fig. 9) correspond to the LP form. At a CO_2 pressure of 0.30 bar, the Bragg peaks due to both the NP and LP forms with equal intensities exist in the XRPD pattern. The intensities of the Bragg peaks of the NP and LP forms remain the same up to a CO_2 pressure of 0.62 bar. At 0.86 bar of CO_2 pressure, the intensities of the Bragg reflections of the LP form become dominant again over those of the NP form, suggesting that the structure is almost re-opened at this CO_2 pressure. The structure is completely re-opened at a CO_2 pressure of 0.95 bar. After that, the sample cell is evacuated and the XRPD pattern of the sample under vacuum consisted of Bragg peaks of only the LP form. This indicates that the structural transition of **2** at −80 °C as a function of CO_2 pressure is reversible.

At −40 °C and a CO_2 pressure of 0.36 bar (Fig. S8, ESI†), the Bragg reflections of a mixture of NP and LP phases are observed in the XRPD pattern of **2**. At a CO_2 pressure of 0.92 bar, a slight increase occurs in the intensity of the Bragg peaks of the LP phase, suggesting that the structure starts to re-open at this CO_2 pressure. At a CO_2 pressure of 1.47 bar, the framework of **2** re-opens completely. After evacuation of CO_2 from the sample cell, the Bragg peaks of only the LP form is visible in the XRPD pattern, thus indicating the reversibility of the structural change of **2** at −40 °C as a function of CO_2 pressure.

Thus, the *in situ* synchrotron XRPD studies demonstrate that the structural transition of **2** occurs at a much lower temperature compared to unfunctionalized Al-MIL-53. Similar lowering of the temperature domain for the structural change has been recently reported for Fe-MIL-53-X (X = –Cl, –Br, $–CH_3$) compared to parent Fe-MIL-53.[26] At both −40 and −80 °C, we were unable to observe a pure NP phase at a certain CO_2 pressure for the determination of unit cell parameters. After keeping the sample at −80 °C for 5 h under vacuum, an almost pure NP phase of **2** was observed and the corresponding XRPD pattern (Fig. S9, ESI†) was used to derive the lattice parameters (Table 1) for the NP phase. It is noteworthy that Al-MIL-53 has been previously reported to undergo similar LP → NP phase transition at the temperature range between −123 and −213 °C.[84]

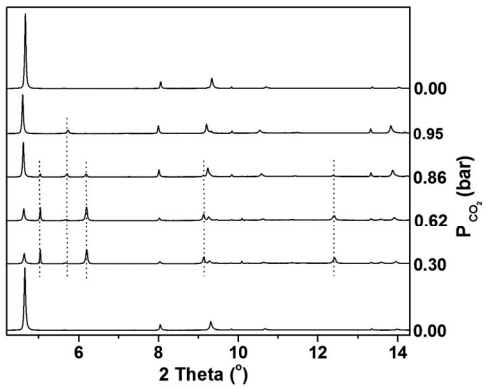

Fig. 9 *In situ* synchrotron XRPD patterns (λ = 0.827131 Å) of **2** collected at a certain pressure of CO_2 and −80 °C. The Bragg peaks marked by dotted lines indicate the narrow pore phase, whereas the rest of the Bragg peaks denote the large pore phase. Before the measurement, the sample was degassed at 200 °C for 30 min under vacuum.

Conclusions

The synthesis, characterization and structural analysis of two new partially fluorinated MOFs, namely MIL-47-F (**1**) and Al-MIL-53-F (**2**), have been demonstrated. The phase purity of the compounds was confirmed by a combination of XRPD analysis, DRIFT spectroscopy, Raman, thermogravimetric and elemental analysis. Thermogravimetric analyses show that **1** and **2** are stable up to 385 and 480 °C, respectively. Remarkably, the thermally activated LP form of **2** upon exposure to air also displays a LP form, which is contrary to unfunctionalized Al-MIL-53 (ref. 28) and other functionalized Al-MIL-53-X (X = –Cl, Br, $–CH_3$, $–NO_2$, $–NH_2$, $–(OH)_2$).[23,66,70] The N_2, CO_2, *n*-hexane, *o*- and *p*-xylene sorption analyses exhibit significant microporosity for both **1** and **2**, which are lower compared to their unfunctionalized analogues. Compared to parent Al-MIL-53, the breathing phenomenon of **2** upon adsorption of *n*-hexane, *o*- and *p*-xylene is dramatically influenced due to functionalization by –F groups. As confirmed by the low-pressure CO_2

sorption and *in situ* synchrotron XRPD analysis as a function of CO_2 pressure, the fluorination also lowers the temperature domain for the structural change of **2** upon adsorption of CO_2, as compared to non-modified Al-MIL-53. The H_2O sorption experiments demonstrate that the fluorination imparts noticeable hydrophobicity to both of the partially fluorinated compounds. Though we were unable to obtain completely hydrophobic MOFs,[59] we believe that the introduction of more –F groups (two or four –F groups per terephthalate linker) will enable the materials to be more hydrophobic and thus enhance the adsorption of linear alkanes or xylenes. Investigations in this direction are in progress in our laboratory and will be reported in due course.

Acknowledgements

This research is funded by Ghent University, GOA grant number 01G00710. Diamond Light Source is acknowledged for providing access to the beamline I11.

References

1 G. Férey, *Chem. Soc. Rev.*, 2008, **37**, 191.
2 S. Kitagawa, R. Kitaura and S. Noro, *Angew. Chem., Int. Ed.*, 2004, **116**, 2388 (*Angew. Chem., Int. Ed.*, 2004, **43**, 2334).
3 O. M. Yaghi, M. O'Keeffe, N. W. Ockwig, H. K. Chae, M. Eddaoudi and J. Kim, *Nature*, 2003, **423**, 705–714.
4 L. J. Murray, M. Dincă and J. R. Long, *Chem. Soc. Rev.*, 2009, **38**, 1294.
5 J.-R. Li, R. J. Kuppler and H.-C. Zhou, *Chem. Soc. Rev.*, 2009, **38**, 1477.
6 L. Hamon, P. L. Llewellyn, T. Devic, A. Ghoufi, G. Clet, V. Guillerm, G. D. Pirngruber, G. Maurin, C. Serre, G. Driver, W. van Beek, E. Jolimaitre, A. Vimont, M. Daturi and G. Férey, *J. Am. Chem. Soc.*, 2009, **131**, 17490.
7 J. Lee, O. K. Farha, J. Roberts, K. A. Scheidt, S. T. Nguyen and J. T. Hupp, *Chem. Soc. Rev.*, 2009, **38**, 1450.
8 L. Ma, C. Abney and W. Lin, *Chem. Soc. Rev.*, 2009, **38**, 1248.
9 K. M. L. Taylor-Pashow, J. Della Rocca, Z. G. Xie, S. Tran and W. B. Lin, *J. Am. Chem. Soc.*, 2009, **131**, 14261.
10 P. Horcajada, T. Chalati, C. Serre, B. Gillet, C. Sebrie, T. Baati, J. F. Eubank, D. Heurtaux, P. Clayette, C. Kreuz, J. S. Chang, Y. K. Hwang, V. Marsaud, Y.-N. Bories, L. Cynober, S. Gil, G. Férey, P. Couvreur and R. Gref, *Nat. Mater.*, 2010, **9**, 172.
11 M. Vallet-Regí, F. Balasm and D. Arcos, *Angew. Chem., Int. Ed.*, 2007, **119**, 7692 (*Angew. Chem., Int. Ed.*, 2007, **46**, 7548).
12 P. Horcajada, C. Serre, M. Vallet-Reg, M. Sebban, F. Taulelle and G. Férey, *Angew. Chem., Int. Ed.*, 2006, **118**, 6120 (*Angew. Chem., Int. Ed.*, 2006, **45**, 5974).
13 K. K. Tanabe and S. M. Cohen, *Chem. Soc. Rev.*, 2011, **40**, 498.
14 G. Férey and C. Serre, *Chem. Soc. Rev.*, 2009, **38**, 1380.
15 M. Eddaoudi, J. Kim, N. Rosi, D. Vodak, J. Wachter, M. O'Keefe and O. M. Yaghi, *Science*, 2002, **295**, 469.
16 C. Yang, X. P. Wang and M. A. Omary, *J. Am. Chem. Soc.*, 2007, **129**, 15454.
17 S. Horike, S. Bureekaew and S. Kitagawa, *Chem. Commun.*, 2008, 471.
18 S. T. Meek, J. J. Perry IV, S. L. Teich-McGoldrick, J. A. Greathouse and M. D. Allendorf, *Cryst. Growth Des.*, 2011, **11**, 4309.
19 F. Debatin, K. Behrens, J. Weber, I. A. Baburin, A. Thomas, J. Schmidt, I. Senkovska, S. Kaskel, A. Kelling, N. Hedin, Z. Bacsik, S. Leoni, G. Seifert, C. Jäger, C. Günter, U. Schilde, A. Friedrich and H.-J. Holdt, *Chem.–Eur. J.*, 2012, **18**, 11630.
20 R. Custelcean and M. G. Gorbunova, *J. Am. Chem. Soc.*, 2005, **127**, 16362.
21 V. Colombo, C. Montoro, A. Maspero, G. Palmisano, N. Masciocchi, S. Galli, E. Barea and J. A. R. Navarro, *J. Am. Chem. Soc.*, 2012, **134**, 12830.
22 M. Kandiah, M. H. Nilsen, S. Usseglio, S. Jakobsen, U. Olsbye, M. Tilset, C. Larabi, E. A. Quadrelli, F. Bonino and K. P. Lillerud, *Chem. Mater.*, 2010, **22**, 6632.
23 S. Biswas, T. Ahnfeldt and N. Stock, *Inorg. Chem.*, 2011, **50**, 9518.
24 T. Devic, P. Horcajada, C. Serre, F. Salles, G. Maurin, B. Moulin, D. Heurtaux, G. Clet, A. Vimont, J.-M. Grenèche, B. Le Ouay, F. Moreau, E. Magnier, Y. Filinchuk, J. Marrot, J.-C. Lavalley, M. Daturi and G. Férey, *J. Am. Chem. Soc.*, 2010, **132**, 1127.
25 P. Horcajada, F. Salles, S. Wuttke, T. Devic, D. Heurtaux, G. Maurin, A. Vimont, M. Daturi, O. David, E. Magnier, N. Stock, Y. Filinchuk, D. Popov, C. Riekel, G. Férey and C. Serre, *J. Am. Chem. Soc.*, 2011, **133**, 17839.
26 T. Devic, F. Salles, S. Bourrelly, B. Moulin, G. Maurin, P. Horcajada, C. Serre, A. Vimont, J.-C. Lavalley, H. Leclerc, G. Clet, M. Daturi, P. L. Llewellyn, Y. Filinchuk and G. Férey, *J. Mater. Chem.*, 2012, **22**, 10266.
27 K. Barthelet, J. Marrot, D. Riou and G. Férey, *Angew. Chem., Int. Ed.*, 2002, **114**, 291 (*Angew. Chem., Int. Ed.*, 2002, **41**, 281).
28 T. Loiseau, C. Serre, C. Huguenard, G. Fink, F. Taulelle, M. Henry, T. Bataille and G. Férey, *Chem.–Eur. J.*, 2004, **10**, 1373.
29 C. Serre, F. Millange, C. Thouvenot, M. Nogues, G. Marsolier, D. Louer and G. Férey, *J. Am. Chem. Soc.*, 2002, **124**, 13519.
30 T. R. Whitfield, X. Wang, L. Liu and A. Jacobson, *Solid State Sci.*, 2005, **7**, 1096.
31 C. Volkringer, T. Loiseau, N. Guillou, G. Férey, E. Elkaim and A. Vimont, *Dalton Trans.*, 2009, 2241.
32 G. Férey, *Chem. Soc. Rev.*, 2008, **37**, 191.
33 F. Millange, N. Guillou, R. I. Walton, J. M. Grenèche, I. Margiolaki and G. Férey, *Chem. Commun.*, 2008, 4732.
34 C. Serre, S. Bourrelly, A. Vimont, N. A. Ramsahye, G. Maurin, P. L. Llewellyn, M. Daturi, Y. Filinchuk, O. Leynaud, P. Barnes and G. Férey, *Adv. Mater.*, 2007, **19**, 2246.

35 A. Boutin, F.-X. Coudert, M.-A. Springuel-Huet, A. V. Neimark, G. Férey and A.-H. Fuchs, *J. Phys. Chem. C*, 2010, **114**, 22237.

36 A. Boutin, S. Couck, F.-X. Coudert, P. Serra-Crespo, J. Gascon, F. Kapteijn, A. H. Fuchs and J. F. M. Denayer, *Microporous Mesoporous Mater.*, 2011, **140**, 108.

37 S. Couck, J. F. M. Denayer, G. V. Baron, T. Rémy, J. Gascon and F. Kapteijn, *J. Am. Chem. Soc.*, 2009, **131**, 6326.

38 V. Finsy, L. Maa, L. Alaerts, D. E. De Vos, G. V. Baron and J. F. M. Denayer, *Microporous Mesoporous Mater.*, 2009, **120**, 221.

39 F. Salles, A. Ghoufi, G. Maurin, R. G. Bell, C. Mellot-Draznieks and G. Férey, *Angew. Chem., Int. Ed.*, 2008, **47**, 8487.

40 E. Stavitski, E. A. Pidko, S. Couck, T. Rémy, E. J. M. Hensen, B. M. Weckhuysen, J. F. M. Denayer, J. Gascon and F. Kapteijn, *Langmuir*, 2011, **27**, 3970.

41 S. Bourrelly, P. L. Llewellyn, C. Serre, F. Millange, T. Loiseau and G. Férey, *J. Am. Chem. Soc.*, 2005, **127**, 13519.

42 P. L. Llewellyn, G. Maurin, T. Devic, S. Loera-Serna, N. Rosenbach, C. Serre, S. Bourrelly, P. Horcajada, Y. Filinchuk and G. Férey, *J. Am. Chem. Soc.*, 2008, **130**, 12808.

43 S. Couck, T. Rémy, G. V. Baron, J. Gascon, F. Kapteijn and J. F. M. Denayer, *Phys. Chem. Chem. Phys.*, 2010, **12**, 9413.

44 P. L. Llewellyn, P. Horcajada, G. Maurin, T. Devic, N. Rosenbach, S. Bourrelly, C. Serre, D. Vincent, S. Loera-Serna, Y. Filinchuk and G. Férey, *J. Am. Chem. Soc.*, 2009, **131**, 13002.

45 T. K. Trung, P. Trens, N. Tanchoux, S. Bourrelly, P. L. Llewellyn, S. Loera-Serna, C. Serre, T. Loiseau, F. Fajula and G. Férey, *J. Am. Chem. Soc.*, 2008, **130**, 16926.

46 T. K. Trung, I. Déroche, A. Rivera, Q. Yang, P. Yot, N. Ramsahye, S. D. Vinot, T. Devic, P. Horcajada, C. Serre, G. Maurin and P. Trens, *Microporous Mesoporous Mater.*, 2011, **140**, 114.

47 N. Rosenbach Jr, A. Ghoufi, I. Déroche, P. L. Llewellyn, T. Devic, S. Bourrelly, C. Serre, G. Férey and G. Maurin, *Phys. Chem. Chem. Phys.*, 2010, **12**, 6428.

48 L. Alaerts, M. Maes, L. Giebeler, P. A. Jacobs, J. A. Martens, J. F. M. Denayer, C. E. A. Kirschhock and D. E. De Vos, *J. Am. Chem. Soc.*, 2008, **130**, 14170.

49 V. Finsy, C. E. A. Kirschhock, G. Vedts, M. Maes, L. Alaerts, D. E. De Vos, G. V. Baron and J. F. M. Denayer, *Chem.–Eur. J.*, 2009, **15**, 7724.

50 H. Leclerc, T. Devic, S. Devautour-Vinot, P. Bazin, N. Audebrand, G. Férey, M. Daturi, A. Vimont and G. Clet, *J. Phys. Chem. C*, 2011, **115**, 19828.

51 P. G. Yot, Q. Ma, J. Haines, Q. Yang, A. Ghoufi, Thomas Devic, C. Serre, V. Dmitriev, G. Férey, C. Zhong and G. Maurin, *Chem. Sci.*, 2012, **3**, 1100.

52 T. Wu, L. Shen, M. Luebbers, C. Hu, Q. Chen, Z. Ni and R. I. Masel, *Chem. Commun.*, 2010, **46**, 6120.

53 C. Yang, X. Wang and M. A. Omary, *J. Am. Chem. Soc.*, 2007, **129**, 15454.

54 Z. Hulvey, D. A. Sava, J. Eckert and A. K. Cheetham, *Inorg. Chem.*, 2011, **50**, 403.

55 Z. Hulvey, E. H. L. Falcao, J. Eckert and A. K. Cheetham, *J. Mater. Chem.*, 2009, **19**, 4307.

56 P. Pachfule, Y. Chen, J. Jiang and R. Banerjee, *Chem.–Eur. J.*, 2012, **18**, 688.

57 P. Pachfule, Y. Chen, S. C. Sahoo, J. Jiang and R. Banerjee, *Chem. Mater.*, 2011, **23**, 2908.

58 S. T. Meek, J. J. Perry IV, S. L. Teich-McGoldrick, J. A. Greathouse and M. D. Allendorf, *Cryst. Growth Des.*, 2011, **11**, 4309.

59 C. Yang, U. Kaipa, Q. Z. Mather, X. Wang, V. Nesterov, A. F. Venero and M. A. Omary, *J. Am. Chem. Soc.*, 2011, **133**, 18094.

60 C. Yang, X. Wang and M. A. Omary, *Angew. Chem., Int. Ed.*, 2009, **121**, 2538.

61 P. Pachfule, R. Das, P. Poddar and R. Banerjee, *Inorg. Chem.*, 2011, **50**, 3855.

62 C. Volkringer, D. Popov, T. Loiseau, G. Férey, M. Burghammer, C. Riekel, M. Haouas and F. Taulelle, *Chem. Mater.*, 2009, **21**, 5695.

63 T. Loiseau, L. Lecroq, C. Volkringer, J. Marrot, G. Férey, M. Haouas, F. Taulelle, S. Bourrelly, P. L. Llewellyn and M. Latroche, *J. Am. Chem. Soc.*, 2006, **128**, 10223.

64 C. Volkringer, D. Popov, T. Loiseau, N. Guillou, G. Férey, M. Haouas, F. Taulelle, C. Mellot-Draznieks, M. Burghammer and C. Riekel, *Nat. Mater.*, 2007, **6**, 760.

65 J. Gascon, U. Aktay, M. D. Hernandez-Alonso, G. P. M. van Klink and F. Kaptejin, *J. Catal.*, 2009, **261**, 75.

66 T. Ahnfeldt, D. Gunzelmann, T. Loiseau, D. Hirsemann, J. Senker, G. Férey and N. Stock, *Inorg. Chem.*, 2009, **48**, 3057.

67 D. Himsl, D. Wallacher and M. Hartmann, *Angew. Chem., Int. Ed.*, 2009, **48**, 4639.

68 C. Volkringer, T. Loiseau, N. Guillou, G. Férey, M. Haouas, F. Taulelle, E. Elkaim and N. Stock, *Inorg. Chem.*, 2010, **49**, 9852.

69 A. Comotti, S. Bracco, P. Sozzani, S. Horike, R. Matsuda, J. Chen, M. Takata, Y. Kubota and S. Kitagawa, *J. Am. Chem. Soc.*, 2008, **130**, 13664.

70 N. Reimer, B. Gil, B. Marszalek and N. Stock, *CrystEngComm*, 2012, **14**, 4119.

71 V. Finsy, H. Verelst, L. Alaerts, D. De Vos, P. A. Jacobs, G. V. Baron and J. F. M. Denayer, *J. Am. Chem. Soc.*, 2008, **130**, 7110.

72 L. Alaerts, C. E. A. Kirschhock, M. Maes, M. A. van der Veen, V. Finsy, A. Depla, J. A. Martens, G. V. Baron, P. A. Jacobs, J. F. M. Denayer and D. E. De Vos, *Angew. Chem., Int. Ed.*, 2007, **46**, 4293.

73 S. T. Meek, J. J. Perry IV, S. L. Teich-McGoldrick, J. A. Greathouse and M. D. Allendorf, *Cryst. Growth Des.*, 2011, **11**, 4309.

74 P.-E. Werner, L. Eriksson and M. Westddahl, *J. Appl. Crystallogr.*, 1985, **18**, 367.

75 A. Boultif and D. J. Louer, *J. Appl. Crystallogr.*, 1991, **24**, 987.
76 *STOE WinXPOW version 2.11*, Stoe & Cie GmbH, Darmstadt, Germany, 2005.
77 A. Centrone, T. Harada, S. Speakman and T. A. Hatton, *Small*, 2010, **6**, 1598.
78 A. V. Neimark, F.-X. Coudert, A. Boutin and A. H. Fuchs, *J. Phys. Chem. Lett.*, 2010, **1**, 445.
79 A. Boutin, F.-X. Coudert, M.-A. Springuel-Huet, A. V. Neimark, G. Férey and A. H. Fuchs, *J. Phys. Chem. C*, 2010, **114**, 22237.
80 K. S. W. Sing, D. H. Everett, R. A. W. Haul, L. Moscou, R. A. Pierotti, J. Rouquerol and T. Siemieniewska, *Pure Appl. Chem.*, 1985, **57**, 603.
81 S. Horike, D. Tanaka, K. Nakagawa and S. Kitagawa, *Chem. Commun.*, 2007, 3395.
82 S. Paranthaman, F.-X. Coudert and A. H. Fuchs, *Phys. Chem. Chem. Phys.*, 2010, **12**, 8123.
83 D. Ma, Y. Li and Z. Li, *Chem. Commun.*, 2011, **47**, 7377.
84 M. Mendt, B. Jee, N. Stock, T. Ahnfeldt, M. Hartmann, D. Himsl and A. Pöppl, *J. Phys. Chem. C*, 2010, **114**, 19443.